Title

Fluidic Device System for Mechanical Processing and Filtering of Human Lipoaspirate Enhances Recovery of Mesenchymal Stem Cells.

Journal

Plastic and reconstructive surgery, 151(1)

ISSN

0032-1052

Authors

Lombardo, Jeremy A
Banyard, Derek A
Widgerow, Alan D
et al.

Publication Date

2023

DOI

10.1097/prs.0000000000009798

Peer reviewed

Fluidic Device System for Mechanical Processing and Filtering of Human Lipoaspirate Enhances Recovery of Mesenchymal Stem Cells

Jeremy A. Lombardo, PhD[1]
Derek A. Banyard, MD, MBA, MS[2,3]
Alan D. Widgerow, MBBCh, MMed[2,3]
Jered B. Haun, PhD[1,4,5,6,7]

Irvine and Orange, CA

Background: Adipose tissue is an easily accessible source of stem and progenitor cells that offers exciting promise as an injectable autologous therapeutic for regenerative applications. Mechanical processing is preferred over enzymatic digestion, and the most common method involves shuffling lipoaspirate between syringes and filtering to produce nanofat. Although nanofat has shown exciting clinical results, the authors hypothesized that new device designs could enhance recovery of stem/progenitor cells through optimization of fluid dynamics principles, integration, and automation.
Methods: The authors designed and fabricated the emulsification and micronization device (EMD) and the filtration device (FD) to replace the manual nanofat procedures. Using human lipoaspirate samples, the EMD and the FD were optimized and compared to traditional nanofat using ex vivo measurements of cell number, viability, and percentage of mesenchymal stem cells and endothelial progenitor cells.
Results: The EMD produced results statistically similar to nanofat, and these findings were confirmed for a cohort of diabetic patients. Combining the FD with the EMD was superior to manually filtered nanofat in terms of both recovered cell percentages (>1.5-fold) and numbers (two- to three-fold). Differences were statistically significant for total mesenchymal stem cells and a $DPP4^{+}/CD55^{+}$ subpopulation linked to improved wound healing in diabetes.
Conclusions: The new EMD and the FD improved mechanical processing of human lipoaspirate in terms of mesenchymal stem cell enrichment and number compared to traditional nanofat. Future work will seek to investigate the wound healing response both in vitro and in vivo, and to refine the technology for automated operation within clinical settings. (*Plast. Reconstr. Surg.* 151: 72e, 2023.)
Clinical Relevance Statement: The new devices improved mechanical processing of human lipoaspirate in terms of stem cell enrichment and number compared to traditional methods. Future work will seek to validate wound healing response and refine the technology for automated operation within clinical settings.

Interest is growing rapidly to use adipose tissue as a potent, easily accessible source of regenerative cells for injectable autologous therapies, as evidenced by the increasing number of clinical trials and commercial isolation systems.[1]

From the [1]Department of Biomedical Engineering, [2]Department of Plastic Surgery, School of Medicine, [3]Center for Tissue Engineering, [4]Department of Chemical and Biomolecular Engineering, [5]Department of Materials Science and Engineering, [6]Chao Family Comprehensive Cancer Center, and [7]Center for Advanced Design and Manufacturing of Integrated Microfluidics, University of California, Irvine.
Received for publication September 22, 2020; accepted January 10, 2022. Accepted for presentation at the 65th Annual Meeting of the Plastic Surgery Research Council, in Toronto, Ontario, May 28 through 31, 2020 (cancelled because of COVID-19).

DOI: 10.1097/PRS.0000000000009798

Disclosure: *Dr. Banyard is co-founder and former chief medical officer at Syntr Health Technologies, Inc., and a paid consultant for Recros Medica, Inc. Dr. Widgerow is chief medical officer of Alastin, Inc., and a royalty recipient of Allergan CA and LITHA Healthcare South Africa but has no conflicting interests with this study. Dr. Haun is chief science officer of Kino Discovery but has no conflicting interests with this study. Dr. Lombardo has no financial interests to disclose.*

This work is supported by THE PLASTIC SURGERY FOUNDATION.

Related digital media are available in the full-text version of the article on www.PRSJournal.com.

Adipose-derived stem cells are a subset of mesenchymal stem cells (MSCs) with adipogenic, osteogenic, and chondrogenic differentiation potential.[2–4] Adipose-derived stem cells have been shown to improve regeneration in bone,[5] cartilage,[6] cardiac tissue,[7] and other organs,[8] and to treat rheumatoid arthritis and Crohn's disease.[9,10] Adipose tissue is obtained by means of tumescent liposuction, and this lipoaspirate is often treated with proteolytic enzymes such as collagenase to release cells that comprise the stromal vascular fraction (SVF). SVF includes mature cells such as fibroblasts, endothelial cells, pericytes, and macrophages; regenerative cells such as MSCs and endothelial progenitor cells (EPCs); and contaminating blood cells. Importantly, SVF has been shown to exhibit comparable regenerative capabilities to adipose-derived stem cells, including improved healing of burns, scars, and ischemic wounds in diabetes and other chronic diseases.[11–17]

Enzymatic digestion of adipose tissue presents regulatory challenges,[18] and may not produce optimal SVF from a therapeutic standpoint. This has led to the development of mechanical methods to liberate SVF without the use of enzymes. A common method involves repeatedly passing lipoaspirate back and forth between two syringes, resulting in an emulsion termed nanofat.[19] After a filtration step, nanofat is injected and has been shown to be effective in correcting superficial rhytides, scars, and discoloration, in addition to improving neovascularization and fat graft survival.[19–21] We recently characterized the cellular composition of nanofat, and demonstrated that stem and progenitor cell populations were enriched by mechanical processing.[22] Specifically, we observed at least three-fold increases in the percentage of MSCs, EPCs, and a subset of MSCs called multilineage differentiating stress-enduring (Muse) cells, which exhibit pluripotency.[23–25] Although these results are exciting, the nanofat method was originally based on standard laboratory supplies and manual steps, and there has been little change to the format. Commercial systems such as the Tulip (Tulip Medical, San Diego, CA) and Lipocube[26] (Lipocube, London, United Kingdom) still require lipoaspirate to be manually pushed by hand between two syringes, with a coupler dictating the effectiveness of micronization. This is followed by a second manual filtering step. Thus, it remains to be seen whether new design concepts can improve the nanofat process. Moreover, automation could reduce variability introduced by human operators. Other mechanical methods have been developed, including centrifuging, shaking, vortexing, and commercial products such as Lipogems (Lipogems International SpA, Milan, Italy).[27–29] However, these methods require even more manual steps and/or laboratory equipment, which is not conducive to clinical settings.

Microfluidic technologies have made it possible to rapidly design and test new concepts for manipulating fluids on the size scale of tissues and cells.[30,31] In previous work, we developed microfluidic device technologies to dissociate tissues into single cells. This included a digestion device to break down tissue using hydrodynamic fluid shear and proteolytic enzymes,[32] a dissociation device to reduce cellular aggregates into single cells using a network of branching channels with repeated expansions and constrictions,[33,34] and a filter device to eliminate remaining aggregates using nylon mesh membranes.[35] We also discovered that the filter device increased cell recovery by two- to three-fold for digested murine kidney, tumor, and liver by means of a dissociation mechanism. Recently, we integrated all three tissue processing technologies into a single platform and demonstrated at least two-fold enhancement of cell recovery for different organs and improved reliability over manual methods.[36] We hypothesized that these results would extend to mechanical processing of human lipoaspirate. Specifically, we hypothesized that the micronization step could be improved by optimally leveraging laminar fluid shear forces to break down tissue and turbulent fluid mixing to emulsify lipid droplets. In addition, integration and replacement of manual steps would improve reliability and lead to the development of a fully automated benchtop system.

In this article, we present a novel fluidic device system for mechanically processing adipose tissue into an injectable therapeutic (Fig. 1). We first designed the emulsification and micronization device (EMD) to enhance mechanical processing relative to the intersyringe method used to produce nanofat. We also designed a new filtration device (FD) to remove the largest adipose tissue fragments from mechanically processed lipoaspirate and to further maximize recovery of stem and progenitor cells. These devices were combined, operated using a pump rather than manual actuation, and processing performance was compared to enzymatic digestion and nanofat processing for stem and progenitor cell recovery.

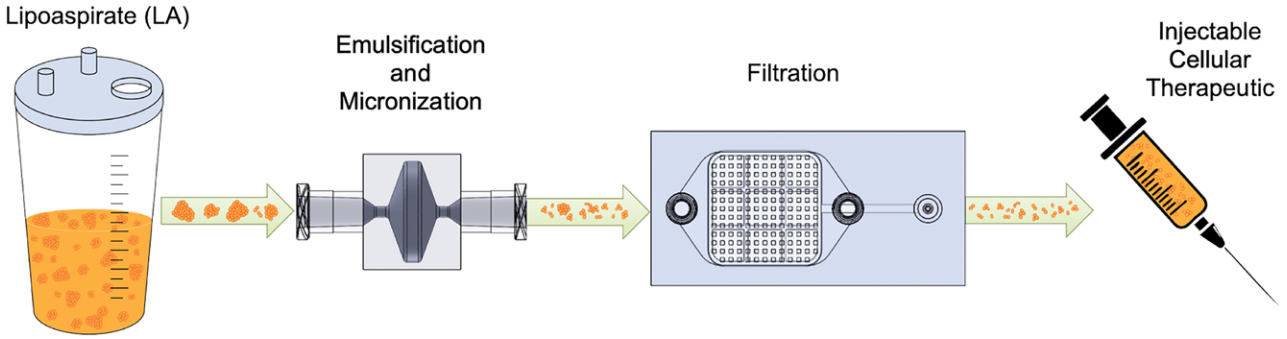

Fig. 1. Fluidic devices for processing adipose tissue. Lipoaspirate is collected by standard vacuum-assisted liposuction and processed using the EMD, which breaks down adipose tissue into smaller fragments and emulsifies fat droplets. The mechanically sheared and emulsified sample is then passed through the FD to remove the largest tissue pieces, which can clog needles during injection. Following device processing, the final cellular suspension can be injected into a patient for augmenting wound healing or other regenerative capacity.

PATIENTS AND METHODS

This study was conducted in accordance with the regulations of the institutional review boards at the University of California, Irvine (no. 2015-2181) and Long Beach VA Hospital (no. 01308). Patients were recruited who were undergoing liposuction for either cosmetic or reconstructive purposes. Active systemic infection or use of immunosuppressive therapy resulted in exclusion from participation. A total of 13 patients were recruited for this study. Four patients had diabetes of unknown type, including two women and two men, with an average age of 61.5 years (range, 59 to 63 years). Both female and male diabetic cohorts were split between those who were African American and White. Nine patients were otherwise healthy, including all women, with an average age of 51.4 years (range, 39 to 76 years). Four were White (44.4%), two were Latina (22.2%), and three were of Asian descent (33.3%). Adipose specimens were collected from the abdomen and/or flanks using standard vacuum-assisted liposuction with a 3- or 3.7-mm harvest cannula and kept at room temperature until use.

EMD Design, Fabrication, and Operation

The EMD features two 1.5-mm-diameter constrictions that are separated by an abrupt expansion (Fig. 2, *above*, *left*). The constrictions generate shear forces that break down tissue into smaller units. Based on the high viscosity of lipoaspirate, we expect laminar flow within the constrictions, which will provide consistent and reliable shear forces for micronization. The rapid expansion is designed to provide turbulent mixing to emulsify the fatty oil layer. Devices were three-dimensionally printed by Dinsmore, Inc. (Irvine, CA) as a single part using an SLA three-dimensional printer and biocompatible Somos BioClear resin (Royal DSM, Elgin, IL). Three-dimensional printing was chosen to produce a single monolithic construct that could withstand high flow rates and pressures required for lipoaspirate processing, during which device clogging is commonly experienced. A fabricated device is shown in Figure 2, *center*, *left*.

The EMD was evaluated using human lipoaspirate samples from otherwise normal ($n = 5$) and diabetic ($n = 4$) patients. Lipoaspirate was washed with phosphate-buffered saline (PBS) and subdivided into separate portions. One portion was left unprocessed and termed macrofat. Another portion was processed into nanofat by manually passing 30 times between two connected syringes, as described previously.[19] Remaining samples were processed with the described method for 10, 20, or 30 passes using a syringe pump (Harvard Apparatus, Holliston, MA) at a flow rate of 20 mL/second, approximately the same flow rate used to manually produce nanofat. We used a high-precision syringe pump to ensure that flow rate was as accurate (within 0.35% of set rate) and reproducible (within 0.05% of actual rate) as possible.

FD Design, Fabrication, and Operation

The FD captures large, millimeter-scale pieces of adipose tissue that remain after processing with the EMD. The multilayer design includes fluidic channels and an embedded nylon mesh membrane (Fig. 2, *right*) that were fabricated by ALine, Inc. (Rancho Dominguez, CA) using a commercial laminate approach, similar to previous work.[35] Membrane pore size was either 0.5 or 1 mm,

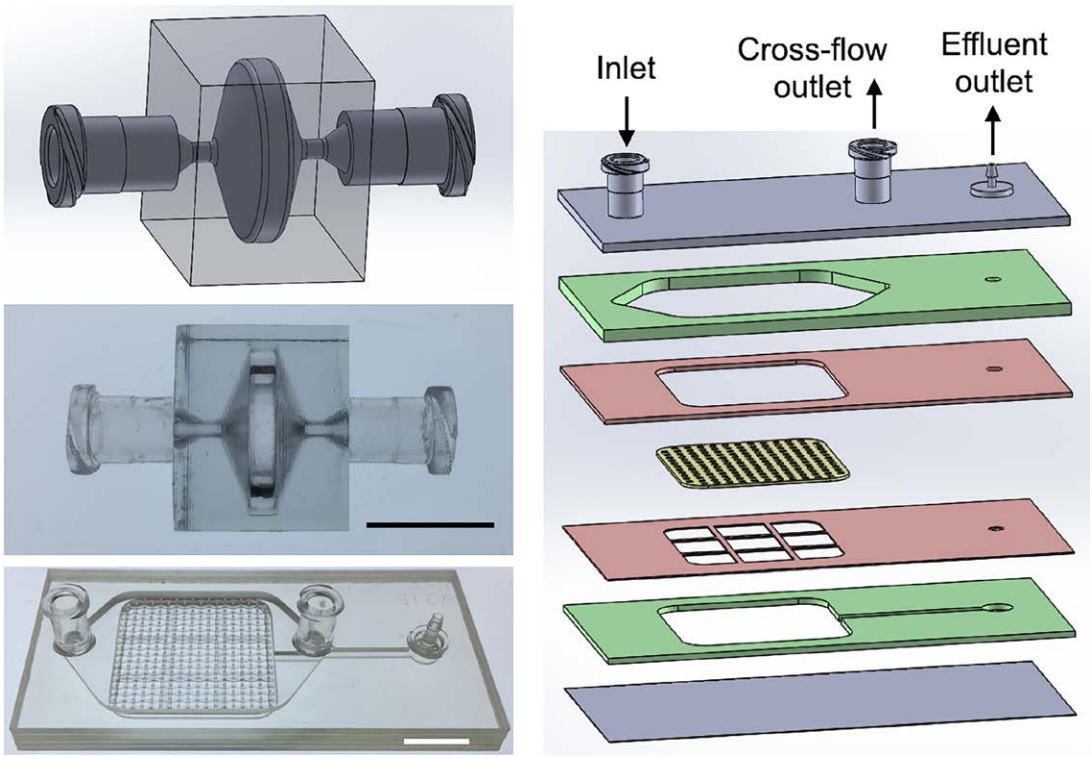

Fig. 2. Processing device design and fabrication. (*Above*, *left* and *center*, *left*) EMD for processing lipoaspirate. (*Above*, *left*) Schematic of design and (*center*, *left*) image of device produced by means of three-dimensional printing. (*Right* and *below*, *left*) FD for removing large tissue fragments after EMD treatment. (*Right*) Exploded view showing six plastic layers, including two for channels (*green*), two acting as the filter spacer and support grid (*red*), and two for sealing the top and bottom of the device. The embedded nylon filter is shown in *yellow*. (*Below*, *left*) Image of the FD with 1-mm-pore nylon filters that was fabricated using pressure lamination. *Scale bars* = 1 cm.

similar to that used to filter nanofat before injection.[19] A fabricated device is shown in Figure 2, *below*, *left*.

Before FD filtration, lipoaspirate from patients (n = 4) was processed using the EMD using 30 passes. Samples were then passed through using a syringe pump at 10 mL/minute. Filtration devices containing either 0.5- or 1-mm nylon mesh membranes were evaluated and compared to nanofat that was passed through a 1-mm mesh cloth. Filtered samples were collected from the effluent outlet.

Cell Isolation

Following mechanical processing, cells were isolated from all samples as described previously.[22] Briefly, 0.1% type I collagenase (Sigma-Aldrich Co., St. Louis, MO) was prepared in PBS, sterilized using a 0.22-μm vacuum filter (Millipore Corp., Billerica, MA), mixed with lipoaspirate at a 1:1 volume ratio, and incubated at 37°C for 30 minutes in a water bath while swirling intermittently. Control medium (Dulbecco's Modified Eagle Medium supplemented with 10% fetal bovine serum, 500 IU penicillin, and 500 μg streptomycin) was then added in an equal volume to neutralize enzymatic activity. The mixture was allowed to separate by gravity for 10 minutes, and the infranatant layer that contains SVF was collected and filtered through a 100-μm cell strainer. Samples were centrifuged at 500 *g* for 7 minutes and pellets were resuspended in control medium. Nucleated cell counts and viability were determined using an automated, dual-fluorescence cell counter (Logos Biosystems, Inc., Annandale, VA).

Flow Cytometry

Collagenase-digested cell suspensions were divided evenly into fluorescence-activated cell sorting tubes and resuspended in fluorescence-activated cell sorting buffer (1× PBS, without calcium and magnesium) supplemented with 1% bovine serum albumin (PBS+). Cell suspensions were stained simultaneously in 100 μl total volume with 5 μl (one test) of each monoclonal mouse anti-human antibody shown in Table 1 (all from

Table 1. Flow Cytometry Probe Panel

Assay	Probe
CD34	Anti-CD34 Ab (clone 561)-BV421
CD45	Anti-CD45 Ab (clone 2D1)-BV510
SSEA-3	Anti-SSEA-3 Ab (clone MC-631)-FITC
CD26	Anti-CD26 Ab (clone BA5b)-PE
CD31	Anti-CD31 Ab (clone WM59)-PE/Cy7
CD55	Anti-CD55 Ab (clone JS11)-APC
CD13	Anti-CD13 Ab (clone WM15)-APC/Cy7
Viability	7-AAD

FITC, fluorescein isothiocyanate; PE, phycoerythrin; APC, allophycocyanin; 7-AAD, 7-aminoactinomycin D.

BioLegend, San Diego, CA). After 20 minutes at 4°C, samples were washed with fluorescence-activated cell sorting buffer by centrifugation, resuspended in PBS+, supplemented with 7-aminoactinomycin D (BD Biosciences, San Jose, CA) for dead cell exclusion, and maintained on ice for at least 15 minutes before analysis on a Novocyte 3000 Flow Cytometer (ACEA Biosciences, San Diego, CA). Compensation was determined using single antibody-stained samples and compensation beads (Invitrogen, Waltham, MA). Heat treatment (55°C for 15 minutes) was used as a dead cell control for 7-aminoactinomycin D. Gates were inputted into FlowJo software (Ashland, OR) to automatically calculate the compensation matrix. Signal positivity was determined using appropriate fluorescence-minus-one controls. A sequential gating scheme was used to identify cell populations of interest from noncellular debris and cellular aggregates. [**See Figure**, **Supplemental Digital Content 1**, which shows the flow cytometry gating scheme. Following mechanical processing, samples were digested with collagenase and cell suspensions were stained with fluorescent probes listed in Table 1 and analyzed using flow cytometry. Acquired data were compensated and assessed using a sequential gating scheme. Gate 1 was used to exclude debris (near origin) based on forward scatter (FSC)-A versus side scatter (SSC)-A. Gate 2 was then used to select single cells based on forward scatter-A versus forward scatter-H. Gate 3 was used to exclude dead cells based on positive 7-aminoactinomycin D signal. Gate 4 was applied to the live cell subset to exclude hematopoietic cells based on positive CD45-BV510 signal. Gate 5 was applied to the CD45– cell subset to identify EPCs based on positive CD34-BV421 and CD31-PE/Cy7 signals, and to identify MSCs based on positive CD34-BV421 and negative CD31-PE/Cy7 signals. Gate 6 was applied to the CD34+, CD31–, MSC subset to identify CD26+(DPP4)/CD55+ cells based on positive CD26-PE and CD55-APC signals. Gate 7 was applied to the CD34+, CD31– MSC subset to identify Muse cells based on positive SSEA3-FITC and CD13-APC/Cy7 signals. Appropriate isotype controls were used to assess nonspecific background staining, and appropriate fluorescence-minus-one controls were used to determine positivity and set gates, ***http://links.lww.com/PRS/F504***.] The cell populations of interest are listed and described in Table 2.

Statistical Analysis

Data are represented as the mean ± standard error from at least three independent patient samples. Statistical analysis included analysis of variance using parametric F tests to evaluate differences between groups and post hoc parametric t tests to evaluate pairwise differences between groups. We also performed nonparametric Kruskal-Wallis tests to confirm that results remained consistent. Differences were considered to be statistically significant when both parametric and nonparametric tests yielded values of $P < 0.05$.

RESULTS

EMD Enriches for MSCs and EPCs in a Similar Manner to Nanofat

We first performed an optimization study for the EMD using human lipoaspirate samples (n = 5 patients) and different numbers of passages through the device at 20 mL/second by means of a syringe pump which demonstrated that 30 produced the best results. [See Figure, **Supplemental Digital Content 2**, which shows the EMD results for all conditions. The results from Figure 3 in the main text are now shown with the EMD optimization tests using 10, 20, and 30 passes. (Above, left) Nucleated cell counts were the same for all EMD pass numbers. (Above, right) Nucleated cell viability remained at approximately 90% for all conditions. (Below) Stem and progenitor

Table 2. Stem and Progenitor Cell Types of Interest

Cell Type	Markers	Significance	References
$CD34^+$	$CD34^+$	Common marker for multipotentiality	38,46
MSCs	$CD45^-$, $CD31^-$, $CD34^+$	Key in regenerative wound healing	47
EPCs	$CD45^-$, $CD31^+$, $CD34^+$	Vascularization of healing tissues	48
Muse	$CD45^-$, $CD31^-$, $CD34^+$, SSEA-3^+, $CD13^+$	Nontumorigenic, pluripotent, stress-tolerant stem cells	23,25
$DPP4^+$/$CD55^+$	$CD45^-$, $CD31^-$, $CD34^+$, $CD26^+$, $CD55^+$	Improved wound healing in diabetic models	24,49

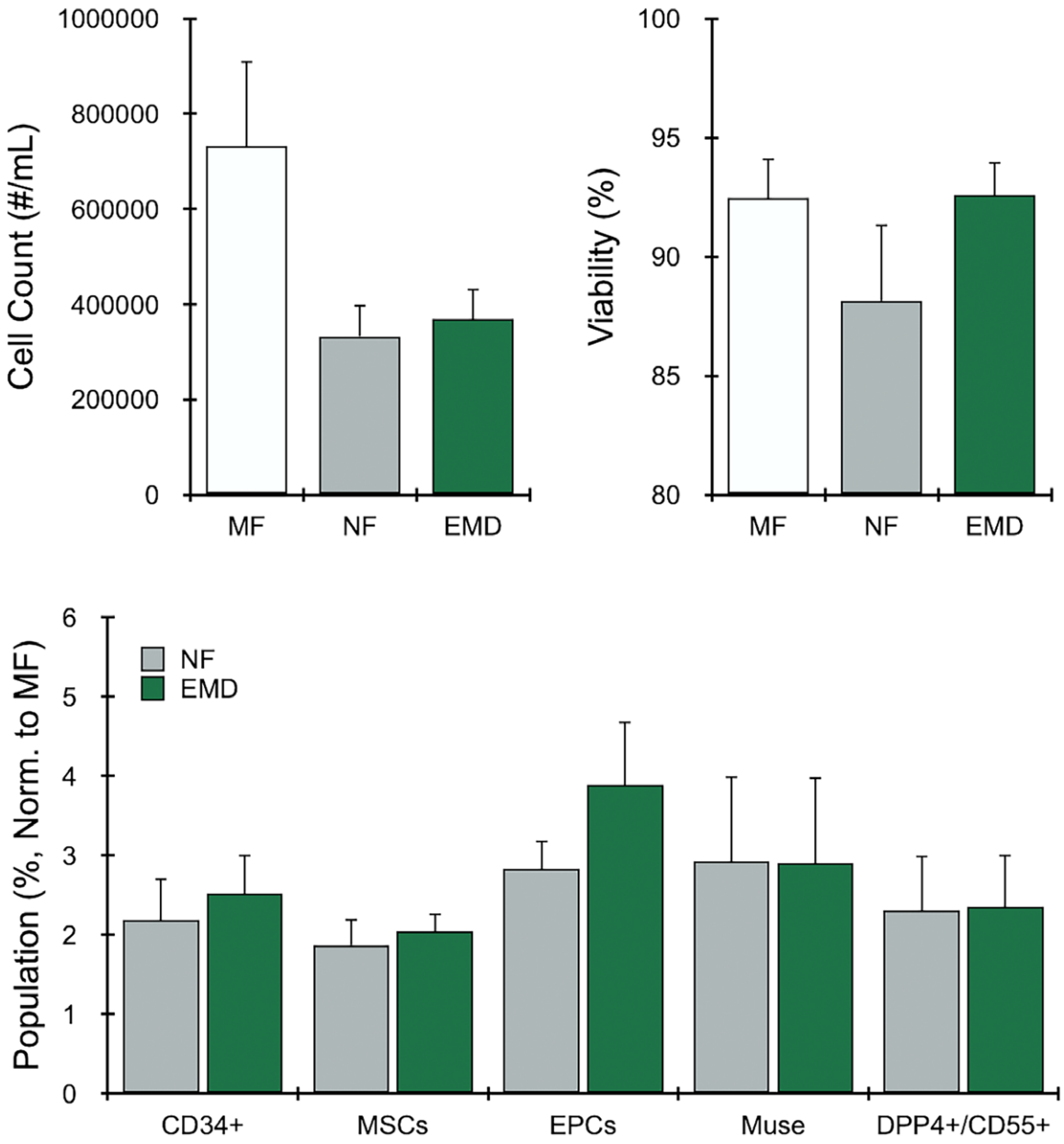

Fig. 3. EMD results for human lipoaspirate. Human lipoaspirate (n = 5) was mechanically processed by manually shuffling between two syringes (nanofat) or using the EMD with 30 device passes. Unprocessed lipoaspirate is indicated as macrofat (*MF*). All samples were digested with collagenase before cell analysis. (*Above*, *left*) Nucleated cell counts decreased by approximately half for nanofat and all device-processed conditions. (*Above*, *right*) Nucleated cell viability remained at approximately 90% for all conditions. (*Below*) Stem and progenitor cells were identified by flow cytometry, and the relative population percentage was calculated and normalized to macrofat (value, 1). Mechanical processing enriched stem/progenitor cell types of interest, often by two- to three-fold compared to macrofat, whereas the EMD provided similar or improved results. *Error bars* = standard error from at least three independent experiments. *NF*, nanofat.

cells enrichment increased in a dose-dependent manner between 10 and 20 passes, but only small changes were observed between 20 and 30 passes. Error bars = standard error from at least three independent experiments. MF, microfat; NF, nanofat; ***http://links.lww.com/PRS/F505***.] Results for this optimal condition are shown in Figure 3, relative to macrofat and nanofat. For total cell recovery, macrofat samples yielded the highest value at approximately 730,000 ± 180,000 cells/

mL of lipoaspirate (Fig. 3, *above*, *left*). Nanofat and EMD produced lower cell counts, by nearly half, but differences were not statistically significant. Viability was similar, at approximately 90%, for all conditions (Fig. 3, *above*, *right*), with no statistically significant differences. The relative percentage of stem/progenitor populations recovered in cell suspensions are shown in Figure 3, *below*. Results were normalized to macrofat because absolute numbers within SVF have been shown to vary widely across different patients and anatomical locations used to harvest adipose tissue.[37,38] Total MSCs, Muse cells and DPP4$^+$/CD55$^+$ MSC subpopulations, and EPCs were all enriched in nanofat, by two- to three-fold, as shown previously.[22] For the EMD, stem/progenitor percentages were generally comparable to nanofat, and differences were not statistically significant. Statistical comparisons for all outcomes and testing conditions are included. (See Table, **Supplemental Digital Content 3**, which shows statistical analysis of EMD processing results shown in Fig. 3 of the main text. MF, microfat; NF, nanofat; ***http://links.lww.com/PRS/F506***.) Population percentage results without normalization to macrofat were similar. [See Figure, **Supplemental Digital Content 4**, which shows the EMD population results without normalization. The results from Fig. 3, below in the main text are now shown without normalizing to macrofat. Population percentages are shown separately for (left) CD34+ cells, (center) MSCs and EPCs, and (right) Muse cells and DPP4+/CD55+ cells. Muse and DPP4+/CD55+ cell percentages, relative to the total MSC population, were consistent across different processing conditions. Thus, differences in these populations shown in Fig. 3, below arose from MSC enrichment shown (center). Error bars = standard error from at least three independent experiments. MF, microfat; NF, nanofat; ***http://links.lww.com/PRS/F507***.]

EMD Enrichment Results Extend to Diabetic Patients

We also evaluated a cohort of diabetic patients (n = 4), and again found that 30 passes through the EMD was optimal. [See Figure, **Supplemental Digital Content 5**, which shows the EMD results for diabetic patients. The results from Fig. 4 in the main text are now shown with the EMD optimization tests using 10, 20, and 30 passes. Results for (left) nucleated cell counts, (center) viability, and (right) normalized cell populations closely followed results in Fig. 3 and Figure, Supplemental Digital Content 2, for normal lipoaspirate samples. Error bars = standard error from at least three independent experiments (*P < 0.05 relative to macrofat by parametric F test). MF, microfat; NF, nanofat, ***http://links.lww.com/PRS/F508***.] Total cell recovery was similar to normal patients (680,000 ± 240,000), with nanofat and the EMD at approximately half of macrofat (Fig. 4, *above*, *left*). These differences were statistically significant based on the parametric F test (P = 0.038), but not the nonparametric Kruskal-Wallis test. Viability was similar for all conditions (Fig. 4, *above*, *right*), with no statistically significant differences. Stem/progenitor cell percentage (Fig. 4, *below*) results followed the initial nondiabetic patient cohort, with all MSC and EPC subtypes enriched by greater than two-fold for both nanofat and the EMD. Statistical comparisons for all outcomes and testing conditions are included. (See Table, **Supplemental Digital Content 6**, which shows statistical analysis of EMD processing results for diabetic patients from Fig. 4 of the main text. MF, microfat; NF, nanofat; ***http://links.lww.com/PRS/F509***.) Nonnormalized population percentages were also similar to the initial nondiabetic patient cohort. [See Figure, **Supplemental Digital Content 7**, which shows the EMD population results for diabetic patients without normalization. The results from Fig. 4, below, in the main text are now shown without normalizing to macrofat. Population percentages are shown separately for (left) CD34+ cells, (center) MSCs and EPCs, and (right) Muse and DPP4+/CD55+ cells. Muse and DPP4+/CD55+ percentages, relative to the total MSC population, were consistent across different processing conditions. Thus, differences in these populations shown in Fig. 4, below arose from MSC enrichment (center). Error bars = standard error from at least three independent experiments. MF, microfat; NF, nanofat; ***http://links.lww.com/PRS/F510***.]

FD Further Enhances Enrichment and Recovery of MSC Populations

Finally, we performed an optimization study for the FD using human lipoaspirate samples (n = 4 patients) and filters with different pore sizes, which indicated that 1-mm pores produced more cells and higher percentages of stem/progenitor cells relative to 0.5 mm. [See Figure, **Supplemental Digital Content 8**, which shows the FD results. The results from Fig. 5 in the main text are now shown with the FD optimization tests using mesh filters with 1- and 0.5-mm pores. (Above, left) Nucleated cell counts decreased after filtering, most notably for nanofat with manual filtering and EMD with the 0.5-mm pores. (Above, right) Nucleated cell viability remained greater than 90% for all

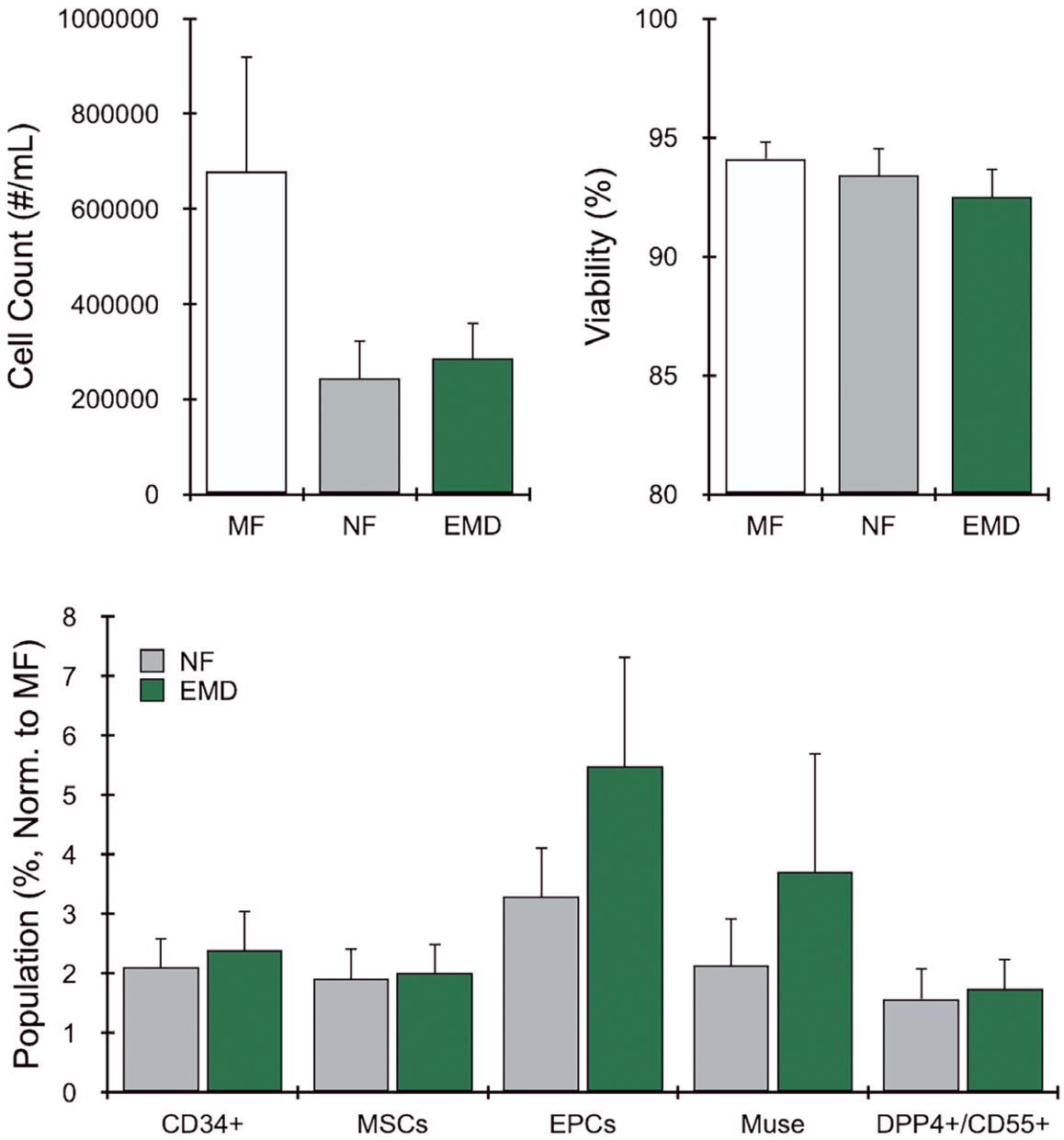

Fig. 4. EMD results for diabetic human lipoaspirate. Diabetic human lipoaspirate ($n = 4$) was mechanically processed as nanofat or the EMD, or left unprocessed as macrofat. All samples were digested with collagenase before cell analysis. Results for (*above*, *left*) nucleated cell counts, (*above*, *right*) viability, and (*below*) normalized cell populations closely followed results in Figure 3 for nondiabetic lipoaspirate samples. *Error bars* = standard error from at least three independent experiments. *MF*, macrofat; *NF*, nanofat.

conditions. The FD with 1-mm membrane better maintained (below, left) enrichment and (below, right) numbers for each cell types from EMD treatment. Error bars = standard error from at least three independent experiments (*P < 0.05 relative to macrofat; **P < 0.01 relative to macrofat; #P < 0.05 relative to nanofat/filter; ##P < 0.01 relative to nanofat/filter by parametric F test). MF, microfat; NF, nanofat; ***http://links.lww.com/PRS/F511***.] Cell recovery for the FD with 1-mm pores was lower than using the EMD alone, but we found that manually filtering nanofat decreased cell recovery and stem/progenitor cell percentages to an even greater extent. Filtered results for nanofat and EMD/FD are shown in Figure 5, relative to macrofat. A total of 900,000 ± 160,000 cells were recovered per milliliter of lipoaspirate from macrofat after enzymatic digestion

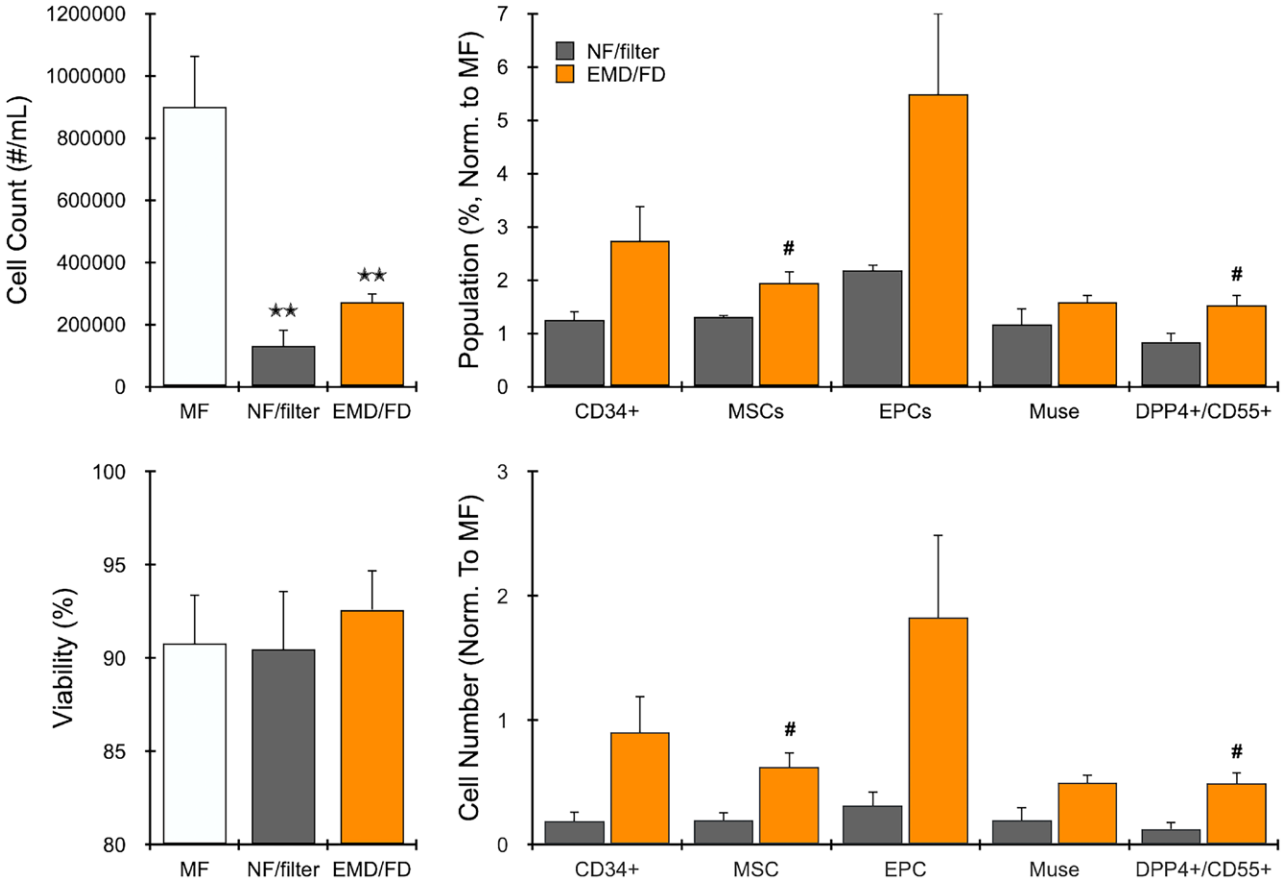

Fig. 5. FD results. Human lipoaspirate ($n = 4$) was mechanically processed as nanofat or using the EMD. Nanofat was then manually filtered using a 1-mm mesh cloth, whereas EMD samples were filtered using the FD with a 1-mm pore size. All samples were digested with collagenase before cell analysis. (*Above*, *left*) Nucleated cell counts decreased by over half for nanofat and EMD–processed samples and further decreased with filtering, most notably for nanofat. (*Below*, *left*) Nucleated cell viability remained greater than 90% for all conditions. (*Above*, *right*) The FD better maintained enrichment of cell types from EMD treatment, with overall higher percentages compared to macrofat (value, 1) and nanofat filtered conditions. (*Below*, *right*) Cell numbers were even greater for EMD/FD relative to filtered nanofat, particularly for total MSCs and the two subpopulations. *Error bars* = standard error from at least three independent experiments (*$P < 0.05$ relative to macrofat; **$P < 0.01$ relative to macrofat; and #$P < 0.05$ relative to nanofat/filter based on both parametric and nonparametric tests). *MF*, macrofat; *NF*, nanofat.

(Fig. 5, *above*, *left*), similar to initial studies. Cell count drastically decreased for manually filtered nanofat to 130,000 ± 50,000 cells/mL, whereas the EMD/FD produced 270,000 ± 30,000 cells/mL. Differences were statistically significant relative to macrofat (F test $P = 0.001$; Kruskal-Wallis test $P = 0.013$). Cell viability remained high, in excess of 90%, for all conditions (Fig. 5, *below*, *left*), with no statistically significant differences. Flow cytometry indicated that much of the stem/progenitor cell enrichment attained by nanofat was lost after filtering (Fig. 4, *below*), with population percentages reduced to near macrofat levels. Conversely, the FD better retained stem/progenitor cell enrichment from EMD conditions, with total $CD34^+$ cells, MSCs, and EPCs all exceeding macrofat by greater than two-fold. Importantly, differences between EMD/FD and filtered nanofat were statistically significant for total MSCs (1.9 ± 0.2 versus 1.3 ± 0.04, F test $P = 0.037$, Kruskal-Wallis test $P = 0.021$) and the $DPP4^+/CD55^+$ MSC subpopulation (1.5 ± 0.2 versus 0.8 ± 0.2, F test $P = 0.039$, Kruskal-Wallis test $P = 0.021$). We also note that additional EMD/FD–processed populations attained statistical significance for one of the tests, but not both, including $CD34^+$ (2.7 ± 0.7 versus 1.2 ± 0.2, F test $P = 0.075$, Kruskal-Wallis test $P = 0.021$) and EPCs (5.5 ± 1.5 versus 2.2 ± 0.1, F test $P = 0.076$, Kruskal-Wallis test $P = 0.021$). [See Figure, **Supplemental Digital Content 9**, which shows the FD population results without normalization. The results from Fig. 5, above, right, in the main text are now shown without normalizing to macrofat. Population percentages are shown

for (left) CD34+ cells, (center) MSCs and EPCs, and (right) Muse and DPP4+/CD55+ cells. Muse and DPP4+/CD55+ percentages, relative to the MSC population, were generally consistent across the different processing conditions. Muse cells were slightly higher and DPP4+/CD55+ cells were slightly lower with mechanical processing, but this difference was not statistically significant. Thus, differences in these populations shown in Fig. 5, above, right, predominantly arose from MSC enrichment. Error bars = standard error from at least three independent experiments (*P < 0.05 relative to macrofat; **P < 0.01 relative to macrofat by parametric F test). MF, microfat; NF, nanofat; ***http://links.lww.com/PRS/F512***.] We note that differences between the EMD/FD and macrofat did reach statistical significance for EPCs following filtration.

We note that the lower cell recovery obtained after filtering nanofat in Figure 5, *above, left,* exacerbates the lower relative number of stem/progenitor cells in Figure 4 (*below*). To illustrate this point, Figure 5 (*below, right*) displays total cell recovery for each stem/progenitor cell type. Results were again normalized to macrofat, which now represents the expected maximum recovery level. Filtered nanofat ranged from 10% to 30% of this recovery potential, whereas the EMD/FD was consistently greater than 50%. EPCs exceeded 100%, but the error was large. Critically, differences between nanofat and EMD/FD reached a high level of statistical significance for MSCs (0.6 ± 0.1 versus 0.2 ± 0.07, *F* test $P = 0.020$, Kruskal-Wallis test $P = 0.021$) and the $DPP4^+/CD55^+$ MSC subpopulation (0.49 ± 0.9 versus 0.12 ± 0.06, *F* test $P = 0.0.104$, Kruskal-Wallis test $P = 0.021$). The other populations attained statistical significance for only one test, including $CD34^+$ (0.9 ± 0.3 versus 0.2 ± 0.1, *F* test $P = 0.0.055$, Kruskal-Wallis test $P = 0.021$), EPCs (1.8 ± 0.7 versus 0.3 ± 0.1, *F* test $P = 0.068$, Kruskal-Wallis test $P = 0.021$), and Muse cells (0.5 ± 0.1 versus 0.2 ± 0.1, *F* test $P = 0.049$, Kruskal-Wallis test $P = 0.083$). Statistical comparisons for all outcomes and testing conditions are provided in Table 3.

DISCUSSION

Human lipoaspirate contains a mixture of non–uniform-sized tissue fragments, cells, and fatty oils that requires both micronization and emulsification. Although the nanofat method has been shown to be effective at processing lipoaspirate into an injectable cellular therapeutic without enzymatic treatment, it requires a sample to be shuffled between two syringes by hand.[19] The EMD was designed to process lipoaspirate in a manner similar to nanofat, but with greater control over flow because of the use of a pump. The design included two constriction regions that were separated by an abrupt expansion, which creates regions of high viscous shear force and turbulent mixing. The EMD resulted in lower total cell recovery relative to macrofat, which was likely caused by destruction of fragile cells by shear forces, as previously observed during nanofat processing.[19] However, stem and progenitor cells appear relatively resistant to these shear forces, leading to enrichment in the cell suspensions.[22] In this study, we found that EMD treatment did result in enrichment of MSCs and EPCs relative to macrofat, statistically similar to nanofat. These results were replicated using lipoaspirate from patients with diabetes. Enrichment of stem/progenitor populations is particularly encouraging in the context

Table 3. Statistical Analysis of EMD and FD Processing Results Shown in Figure 5

Outcomes	Mean ± SD			Parametric *F* Test *P*	Post Hoc *t* Tests			Nonparametric Kruskal-Wallis Test *P*
	MF	NF	EMD		EMD vs.MF	EMD vs.NF	NF vs.MF	
Count	898,525 ± 329,107	130,613 ± 103,428	271,450 ± 58,106	0.0010	0.0045	0.6032	0.0012	0.0125
Viability	90.8 ± 5.2	90.5 ± 6.3	92.6 ± 4.2	0.8330	0.8823	0.8406	0.9959	0.7939
Population (%, normalized to MF)								
CD34		1.2 ± 0.3	2.7 ± 1.3	0.0745		0.0745		0.0209
MSCs		1.3 ± 0.1	1.9 ± 0.5	0.0373		0.0373		0.0209
EPCs		2.2 ± 0.2	5.5 ± 3.1	0.0755		0.0755		0.0209
Muse		1.2 ± 0.6	1.6 ± 0.3	0.2580		0.2580		0.3865
DPP4		0.8 ± 0.4	1.5 ± 0.4	0.0393		0.0393		0.0209
Cell number (normalized to MF)								
CD34		0.2 ± 0.2	0.9 ± 0.6	0.0552		0.0552		0.0209
MSCs		0.2 ± 0.1	0.6 ± 0.2	0.0197		0.0197		0.0209
EPCs		0.3 ± 0.2	1.8 ± 1.3	0.0676		0.0676		0.0209
Muse		0.2 ± 0.2	0.5 ± 0.1	0.0488		0.0488		0.0833
DPP4		0.1 ± 0.1	0.5 ± 0.2	0.0139		0.0139		0.0209

MF, macrofat; NF, nanofat.

of diabetes, as wound healing and neovascularization are well known to be impaired.[39] Specifically, diabetes has been shown to deplete key stem cell subpopulations in adipose tissue,[40] which highlights the potential impact of enhanced enrichment and recovery.[41]

The FD was designed to work in concert with the EMD, removing any remaining large, millimeter-scale pieces of adipose tissue that would not be able to pass through small-bore needles. The FD better preserved both total cell recovery and stem/progenitor enrichment in comparison to nanofat with manual filtration. Specifically, the FD containing a 1-mm membrane produced greater than two-fold more total cells and greater enrichment levels for all stem/progenitor cells studied. Most importantly, these two effects combined to increase the total number of stem/progenitor cells recovered, and this difference was statistically significant for total MSCs and the $DPP4^+/CD55^+$ subpopulation, whereas Muse and EPCs were at the borderline of significance. This implies that most nanofat-processed cells are lost during the filtration step, and thus excluded from the final injectable therapeutic. Conversely, two- to three-fold more stem/progenitors will be present in cell suspensions generated with the EMD/FD. Interestingly, we found that EPCs were higher after EMD/FD treatment in comparison to macrofat, which should not be possible because macrofat was not filtered. This difference was not significant, but it could suggest that our fluidic device system is more effective at dissociating tissues than enzymatic treatment alone, as we have observed in our previous work.[32,42–44] We will follow up on this finding in future studies.

We acknowledge that the strongest effect that we observed in this study was for the FD following EMD treatment. We suspect that enhanced processing by the EMD played a role, but at this time, we do not know whether the FD would similarly improve cell recovery for nanofat. It is also unclear how the FD would compare to commercial filtration systems such as the Tulip and Lipocube following either EMD or nanofat.[26] These questions will all be studied in future work. We do note that our results were obtained using a syringe pump, obviating the need for manual contribution from a human operator, which can introduce variability, and in general presents a challenge to generating consistent and reproducible flow rates and shear forces. This could, in turn, negatively affect the quality of the final cell suspension. Migrating to a pump-driven system will help to standardize and automate the processing of lipoaspirate for clinical settings. Our EMD and FD technologies were designed to function as disposable cartridges for such an automated system, which will be developed and tested in future work.

Limitations to this study include patient-to-patient variability with respect to the number of cells recovered from lipoaspirate for various cell subpopulations. Although macrofat normalization did provide clear evidence of the effects of mechanical processing and filtration, we will seek to confirm these findings in larger cohorts, including patients with both type 1 and type 2 diabetes. Notably, we have only assessed stem/progenitor cell enrichment and recovery number, and thus future work will seek to directly assess prohealing responses in vitro, using animal models, and, after obtaining regulatory approval, in human subjects. Finally, we have focused on injectable cellular therapeutics, but nanofat has also been explored for fat grafting, and it has been shown that downstream processing such as staged centrifugation can concentrate MSCs.[45] Alternative processing methods and applications, such as fat grafting, will be investigated in future studies.

CONCLUSIONS

In this work, we have presented and characterized a set of new fluidic devices that mechanically processes human lipoaspirate by means of emulsification, micronization, and filtering into a format that can be injected directly as a cell-based therapeutic. This system is similar to nanofat, but significantly enhances MSCs and EPCs in terms of cell numbers and relative concentration. Fluid is also driven using a pump instead of manual actuation, which holds the potential for automating and standardizing lipoaspirate processing in the clinical setting. Future work will seek to evaluate whether the findings here translate to improved wound healing using in vitro and in vivo models, and to develop an automated benchtop system.

Jered B. Haun, PhD
Department of Biomedical Engineering
University of California, Irvine
3107 Natural Sciences II
Irvine, CA 92697
jered.haun@uci.edu

DISCLAIMER

The content is solely the responsibility of the authors and does not necessarily represent the official views of the National Institutes of Health or the Plastic Surgery Foundation.

ACKNOWLEDGMENTS

Funding support was received from the National Center for Research Resources and the National Center for Advancing Translational Sciences, National Institutes of Health, through Grant UL1 TR001414, and the Plastic Surgery Foundation through the National Endowment for Plastic Surgery Grant PSF-207585. The authors would like to thank Keyianoosh Paydar, MD, Garrett Wirth, MD, and the Department of Plastic Surgery, University of California, Irvine, for support and assistance with specimen collection. They also thank Tuyen Hoang, PhD, of the Biostatistics, Epidemiology, and Research Design Unit of the Institute for Clinical and Translational Sciences for performing statistical analyses.

REFERENCES

1. Chu DT, Nguyen Thi Phuong T, Tien NLB, et al. Adipose tissue stem cells for therapy: an update on the progress of isolation, culture, storage, and clinical application. *J Clin Med.* 2019;8:917.
2. Zuk PA, Zhu M, Mizuno H, et al. Multilineage cells from human adipose tissue: implications for cell-based therapies. *Tissue Eng.* 2001;7:211–228.
3. Bunnell BA, Flaat M, Gagliardi C, Patel B, Ripoll C. Adipose-derived stem cells: isolation, expansion and differentiation. *Methods* 2008;45:115–120.
4. Gimble JM, Katz AJ, Bunnell BA. Adipose-derived stem cells for regenerative medicine. *Circ Res.* 2007;100:1249–1260.
5. Godoy Zanicotti D, Coates DE, Duncan WJ. In vivo bone regeneration on titanium devices using serum-free grown adipose-derived stem cells, in a sheep femur model. *Clin Oral Implants Res.* 2017;28:64–75.
6. Latief N, Raza FA, Bhatti FU, Tarar MN, Khan SN, Riazuddin S. Adipose stem cells differentiated chondrocytes regenerate damaged cartilage in rat model of osteoarthritis. *Cell Biol Int.* 2016;40:579–588.
7. Valina C, Pinkernell K, Song YH, et al. Intracoronary administration of autologous adipose tissue-derived stem cells improves left ventricular function, perfusion, and remodelling after acute myocardial infarction. *Eur Heart J.* 2007;28:2667–2677.
8. Frese L, Dijkman PE, Hoerstrup SP. Adipose tissue-derived stem cells in regenerative medicine. *Transfus Med Hemother.* 2016;43:268–274.
9. De Francesco F, Romano M, Zarantonello L, et al. The role of adipose stem cells in inflammatory bowel disease: from biology to novel therapeutic strategies. *Cancer Biol Ther.* 2016;17:889–898.
10. Garimella MG, Kour S, Piprode V, et al. Adipose-derived mesenchymal stem cells prevent systemic bone loss in collagen-induced arthritis. *J Immunol.* 2015;195:5136–5148.
11. Nguyen A, Guo J, Banyard DA, et al. Stromal vascular fraction: a regenerative reality? Part 1: Current concepts and review of the literature. *J Plast Reconstr Aesthet Surg.* 2016;69:170–179.
12. Guo J, Nguyen A, Banyard DA, et al. Stromal vascular fraction: a regenerative reality? Part 2: Mechanisms of regenerative action. *J Plast Reconstr Aesthet Surg.* 2016;69:180–188.
13. Cianfarani F, Toietta G, Di Rocco G, Cesareo E, Zambruno G, Odorisio T. Diabetes impairs adipose tissue-derived stem cell function and efficiency in promoting wound healing. *Wound Repair Regen.* 2013;21:545–553.
14. Han S, Sun HM, Hwang KC, Kim SW. Adipose-derived stromal vascular fraction cells: update on clinical utility and efficacy. *Crit Rev Eukaryot Gene Expr.* 2015;25:145–152.
15. Semon JA, Zhang X, Pandey AC, et al. Administration of murine stromal vascular fraction ameliorates chronic experimental autoimmune encephalomyelitis. *Stem Cells Transl Med.* 2013;2:789–796.
16. Lee HC, An SG, Lee HW, et al. Safety and effect of adipose tissue-derived stem cell implantation in patients with critical limb ischemia: a pilot study. *Circ J.* 2012;76:1750–1760.
17. Atalay S, Coruh A, Deniz K. Stromal vascular fraction improves deep partial thickness burn wound healing. *Burns* 2014;40:1375–1383.
18. Banyard DA, Salibian AA, Widgerow AD, Evans GR. Implications for human adipose-derived stem cells in plastic surgery. *J Cell Mol Med.* 2015;19:21–30.
19. Tonnard P, Verpaele A, Peeters G, Hamdi M, Cornelissen M, Declercq H. Nanofat grafting: basic research and clinical applications. *Plast Reconstr Surg.* 2013;132:1017–1026.
20. Uyulmaz S, Sanchez Macedo N, Rezaeian F, Giovanoli P, Lindenblatt N. Nanofat grafting for scar treatment and skin quality improvement. *Aesthet Surg J.* 2018;38:421–428.
21. Yu Q, Cai Y, Huang H, et al. Co-transplantation of nanofat enhances neovascularization and fat graft survival in nude mice. *Aesthet Surg J.* 2018;38:667–675.
22. Banyard DA, Sarantopoulos CN, Borovikova AA, et al. Phenotypic analysis of stromal vascular fraction after mechanical shear reveals stress-induced progenitor populations. *Plast Reconstr Surg.* 2016;138:237e–247e.
23. Heneidi S, Simerman AA, Keller E, et al. Awakened by cellular stress: isolation and characterization of a novel population of pluripotent stem cells derived from human adipose tissue. *PLoS One* 2013;8:e64752.
24. Kinoshita K, Kuno S, Ishimine H, et al. Therapeutic potential of adipose-derived SSEA-3-positive Muse cells for treating diabetic skin ulcers. *Stem Cells Transl Med.* 2015;4:146–155.
25. Ogura F, Wakao S, Kuroda Y, et al. Human adipose tissue possesses a unique population of pluripotent stem cells with nontumorigenic and low telomerase activities: potential implications in regenerative medicine. *Stem Cells Dev.* 2014;23:717–728.
26. Tiryaki KT, Cohen S, Kocak P, Turkay SC, Hewett S. In-vitro comparative examination of the effect of stromal vascular fraction isolated by mechanical and enzymatic methods on wound healing. *Aesthet Surg J.* 2020;40:1232–1240.
27. Aronowitz JA, Lockhart RA, Hakakian CS. Mechanical versus enzymatic isolation of stromal vascular fraction cells from adipose tissue. *Springerplus* 2015;4:713.
28. Ghiasloo M, Lobato RC, Díaz JM, Singh K, Verpaele A, Tonnard P. Expanding clinical indications of mechanically isolated stromal vascular fraction: a systematic review. *Aesthet Surg J.* 2020;40:NP546–NP560.
29. Tremolada C, Colombo V, Ventura C. Adipose tissue and mesenchymal stem cells: state of the art and Lipogems technology development. *Curr Stem Cell Rep.* 2016;2:304–312.
30. Duncombe TA, Tentori AM, Herr AE. Microfluidics: reframing biological enquiry. *Nat Rev Mol Cell Biol.* 2015;16:554–567.
31. El-Ali J, Sorger PK, Jensen KF. Cells on chips. *Nature* 2006;442:403–411.
32. Qiu X, Westerhof TM, Karunaratne AA, et al. Microfluidic device for rapid digestion of tissues into cellular suspensions. *Lab Chip* 2017;17:3300–3309.

33. Qiu X, De Jesus J, Pennell M, Troiani M, Haun JB. Microfluidic device for mechanical dissociation of cancer cell aggregates into single cells. *Lab Chip* 2015;15:339–350.
34. Qiu X, Huang JH, Westerhof TM, et al. Microfluidic channel optimization to improve hydrodynamic dissociation of cell aggregates and tissue. *Sci Rep*. 2018;8:2774.
35. Qiu X, Lombardo JA, Westerhof TM, et al. Microfluidic filter device with nylon mesh membranes efficiently dissociates cell aggregates and digested tissue into single cells. *Lab Chip* 2018;18:2776–2786.
36. Lombardo JA, Aliaghaei M, Nguyen QH, Kessenbrock K, Haun JB. Microfluidic platform accelerates tissue processing into single cells for molecular analysis and primary culture models. *Nat Commun*. 2021;12:2858.
37. Jurgens WJ, Oedayrajsingh-Varma MJ, Helder MN, et al. Effect of tissue-harvesting site on yield of stem cells derived from adipose tissue: implications for cell-based therapies. *Cell Tissue Res*. 2008;332:415–426.
38. Philips BJ, Grahovac TL, Valentin JE, et al. Prevalence of endogenous CD34+ adipose stem cells predicts human fat graft retention in a xenograft model. *Plast Reconstr Surg*. 2013;132:845–858.
39. Brem H, Tomic-Canic M. Cellular and molecular basis of wound healing in diabetes. *J Clin Invest*. 2007;117:1219–1222.
40. Rennert RC, Sorkin M, Januszyk M, et al. Diabetes impairs the angiogenic potential of adipose-derived stem cells by selectively depleting cellular subpopulations. *Stem Cell Res Ther*. 2014;5:79.
41. Thomas S, Widgerow AD, Lakey JRT, et al. Adipose derived stem cells and wound healing in patients with diabetes: a promising therapeutic modality. *CellR4* 2014;2:e1309.
42. Qiu X, De Jesus J, Pennell M, Troiani M, Haun JB. Microfluidic device for mechanical dissociation of cancer cell aggregates into single cells. *Lab Chip* 2015;15:339–350.
43. Qiu X, Huang JH, Westerhof TM, et al. Microfluidic channel optimization to improve hydrodynamic dissociation of cell aggregates and tissue. *Sci Rep*. 2018;8:2774.
44. Qiu X, Lombardo JA, Westerhof TM, et al. Microfluidic filter device with nylon mesh membranes efficiently dissociates cell aggregates and digested tissue into single cells. *Lab Chip* 2018;18:2776–2786.
45. Pallua N, Grasys J, Kim BS. Enhancement of progenitor cells by two-step centrifugation of emulsified lipoaspirates. *Plast Reconstr Surg*. 2018;142:99–109.
46. Sidney LE, Branch MJ, Dunphy SE, Dua HS, Hopkinson A. Concise review: evidence for CD34 as a common marker for diverse progenitors. *Stem Cells* 2014;32:1380–1389.
47. Murphy MB, Moncivais K, Caplan AI. Mesenchymal stem cells: environmentally responsive therapeutics for regenerative medicine. *Exp Mol Med*. 2013;45:e54.
48. Chong MS, Ng WK, Chan JK. Concise review: endothelial progenitor cells in regenerative medicine. Applications and challenges. *Stem Cells Transl Med*. 2016;5:530–538.
49. Rennert RC, Januszyk M, Sorkin M, et al. Microfluidic single-cell transcriptional analysis rationally identifies novel surface marker profiles to enhance cell-based therapies. *Nat Commun*. 2016;7:11945.